Research Article | Vol. 8, No. 3 | 1 Mar 2017 | BIOMEDICAL OPTICS EXPRESS 1390
Biomedical Optics EXPRESS

Chemical basis for alteration of an intraocular lens using a femtosecond laser

JOSEF F. BILLE,[1,2,*] JOHANN ENGELHARDT,[3] HANS-ROBERT VOLPP,[4] ABDELMOUTALIB LAGHOUISSA,[4] MARCUS MOTZKUS,[4] ZHONGXIANG JIANG,[5] AND RUTH SAHLER[1]

[1]*Perfect Lens, LLC, 17785 Sky Park Circle Ste.B, Irvine, CA 92614, USA*
[2]*University of Heidelberg, Heidelberg 69120, Germany*
[3]*German Cancer Research Center (DKFZ), BioQuant (INF 267), Im Neuenheimer Feld 280, Heidelberg 69120, Germany*
[4]*Physikalisch-Chemisches Institut, Im Neuenheimer Feld 280/229, University of Heidelberg, Heidelberg 69120, Germany*
[5]*Leica Microsystems CMS GmbH, Am Friedensplatz 3, Mannheim 68165, Germany*
[*]*josef.bille@urz.uni-heidelberg.de*

Abstract: The chemical basis for the alteration of the refractive properties of an intraocular lens with a femtosecond laser was investigated. Three different microscope setups have been used for the study: Laser Induced Fluorescence (LIF) microscopy, Raman microscopy and coherent anti-Stokes Raman Scattering (CARS) microscopy. Photo-induced hydrolysis of polymeric material in aqueous media produces two hydrophilic functional groups: acid group and alcohol group. The spectral signatures identify two of the hydrophilic polar molecules as N-phenyl-4-(phenylazo)-benzenamine ($C_{18}H_{15}N_3$) and phenazine-1-carboxylic acid ($C_{13}H_8N_2O_2$). The change in hydrophilicity results in a negative refractive index change in the laser-treated areas.

OCIS codes: (170.0170) Medical optics and biotechnology; (170.4470) Ophthalmology; (170.6280) Spectroscopy, fluorescence and luminescence.

References and links

1. Y. Ohmachi and T. Igo, "Laser-Induced Refractive-Index Change in As–S–Ge Glasses," Appl. Phys. Lett. **20**(12), 506–508 (1972).
2. L. Ding, R. Blackwell, J. F. Kunzler, and W. H. Knox, "Large refractive index change in silicone-based and non-silicone-based hydrogel polymers induced by femtosecond laser micro-machining," Opt. Express **14**(24), 11901–11909 (2006).
3. L. Ding, "Micro-processing of Polymers and Biological Materials Using High Repetition Rate Femtosecond Laser Pulses," (Ph.D. Thesis), University of Rochester, New York, United States (2009).
4. N. Takeshima, Y. Kuroiwa, Y. Narita, S. Tanaka, and K. Hirao, "Fabrication of a periodic structure with a high refractive-index difference by femtosecond laser pulses," Opt. Express **12**(17), 4019–4024 (2004).
5. S. Katayama and M. Horiike, "Plastic Object,"U.S. Patent Application Publication 2002/0117624 (2002).
6. R. Sahler, S. Q. Zhou, and J. F. Bille, "Hydrophilicity alteration system and method,"U.S patent 9186242 B2 (2015).
7. R. Sahler, J. F. Bille, S. Enright, S. Chhoeung, and K. Chan, "Creation of a refractive lens within an existing intraocular lens using a femtosecond laser," J. Cataract Refract. Surg. **42**(8), 1207–1215 (2016).
8. R. Sahler, J. F. Bille, and D. Schanzlin, "In Vivo IOL modification," https://millennialeye.com/articles/2016-nov-dec/in-vivo-iol-modification
9. G. Bracco and B. Holst, *Surface Science Techniques* (Springer-Verlag Berlin Heidelberg, 2013).
10. F. Görlitz, "P. Hoyer P, HJ Falk,L. Kastrup, J Engelhardt, and SW Hell, "A STED Microscope Designed for Routine Biomedical Applications," Prog. Electromagnetics Res. **147**(April), 57–68 (2014).
11. Technical Manual, "XploRATM Plus System," http://www.horiba.com/fileadmin/uploads/Scientific/Documents/Raman/Brochure_XploRA_Series-062016-B.pdf
12. Leica MicroSystems CMS GmbH, "TCS SP8 Confocal Microscope," http://passthrough.fw-notify.net/download/857371/http://www.well.ox.ac.uk/_asset/file/lecia-sp8-confocal-user-manual.pdf
13. Carl Zeiss Meditec, Jena, "Hydrophilic IOLs," http://www.zeiss.ph/C125679E00525939/EmbedTitelIntern/hydrophil_acryl_hapticdesign_eng/$File/hydrophil_acryl_hapticdesign_eng.pdf

#283250 https://doi.org/10.1364/BOE.8.001390
Journal © 2017 Received 26 Dec 2016; revised 31 Jan 2017; accepted 2 Feb 2017; published 6 Feb 2017

Biomedical Optics EXPRESS

14. Carl Zeiss Meditec, Jena, "Hydrophobic IOLs," https://www.zeiss.com/meditec/int/products/ophthalmology-optometry/cataract/iol-implantation/hydrophobic-c-loop-iols/ct-lucia.html#technical-data
15. AMO, Santa Ana, "Hydrophobic IOLs," https://www.abbottmedicaloptics.com/pdf/TECNIS_One_Piece_Insert.pdf
16. Z. K. Wang, H. Y. Zheng, C. P. Lim, and Y. C. Lam, "Polymer hydrophilicity and hydrophobicity induced by femtosecond laser direct irradiation," Appl. Phys. Lett. **95**(11), 111110 (2009).
17. C. Wochnowski, M. A. Shams Eldin, and S. Metev, "UV-laser-assisted degradation of poly (methyl methacrylate)," Polym. Degrad. Stabil. **89**(2), 252–264 (2005).
18. E. Kemal and S. Deb, "Design and synthesis of three-dimensional hydrogel scaffolds for intervertebral disc repair," J. Mater. Chem. **22**(21), 10725–10734 (2012).
19. T. S. Perova, J. K. Vij, and H. Xu, "Fourier transform infrared study of poly (2-hydroxyethyl methacrylate) PHEMA," Colloid Polym. Sci. **275**(4), 323–332 (1997).
20. A. Bertoluzza, P. Monti, J. V. Garcia-Ramos, R. Simoni, R. Caramazza, and A. Calzavara, "Applications of Raman spectroscopy to the ophthalmological field: Raman spectra of soft contact lenses made of poly-2-hydroxyethylmethacrylate (PHEMA)," J. Molecular Structure **143**(1–2), 469–472 (1986).
21. T. Werner, "Triplet Deactivation in Benzotriazole-Type Ultraviolet Stabilizers," The Journal of Physical Chemistry, Vol. **83**(3), 320–325 (1979).
22. P. M. Miladinova and T. N. Konstantinova, "Photostabilizers for Polymers - New Trends," J. Chemical Technology and Metallurgy **50**(3), 229–239 (2015).
23. G. Mabilleau, C. Cincu, M. F. Baslé, and D. Chappard, "Polymerization of 2-(hydroxyethyl) methacrylate by two different initiator/accelerator systems: a Raman spectroscopic monitoring," J. Raman Spectrosc. **39**(7), 767–771 (2008).
24. J. B. Lonzaga, S. M. Avaneysyan, S. C. Langford, and J. T. Dickinson, "Color center formation in soda-lime glass with femtosecond laser pulses," J. Appl. Phys. **94**(7), 4332–4340 (2003).
25. S. M. Avanesyan, S. Orlando, C. Langford, and J. T. Dickinson, "Generation of color centers by femtosecond laser pulses in wide band gap materials," Proc. SPIE **5352**, 169–179 (2004).
26. S. M. Eaton, G. Cerullo, and R. Osellame, "Fundamentals of Femtosecond Laser Modification of Bulk Dielectrics (Chapter 1)," in R. Osellame et al (Eds.), *Femtosecond Laser Micromachining, Topics in Applied Physics* **123**, (Springer-Verlag Berlin Heidelberg, 2012) pp. 3–18.
27. L. Courrol, R. Samad, L. Gomez, I. Ranieri, S. Baldochi, A. Zanardi de Freitas, and N. Vieira, Junior., "Color center production by femtosecond pulse laser irradiation in LiF crystals," Opt. Express **12**(2), 288–293 (2004).
28. F. Vega, J. Armengol, V. Diez-Blanco, J. Siegel, J. Solis, B. Barcones, A. Pérez-Rodriguez, and P. Loza-Alvarez, "Mechanism of refractive index modification during femtosecond laser writing of waveguides in alkaline lead-oxide silicate glass," Appl. Phys. Lett. **87**(2), 021109 (2005).
29 R.R. Gattas and E. Mazur, "Femtosecond laser micromachining in transparent materials," Nature Photonics **2**, 219–225 (2008).
30. K. Sugioka and Y. Cheng, "Ultrafast lasers – reliable tools for advanced materials processing," Light Sci. Appl. **3**(4), e149 (2014).

1. Introduction

The use of the femtosecond laser to create refractive index change in various materials has been studied for years. Ohmachi et al. (1972) showed a refractive index change of 0.056 in glass using a femtosecond laser [1]. Ding (2006) used a femtosecond laser to obtain a refractive index change of up to 0.06 in hydrogel polymers [2].

Different theories regarding femtosecond laser material interactions which affect the refractive index change have been offered. The Rochester Group hypothesized that the light from the femtosecond laser induced crosslinking within a hydrophilic material and thus created an increase in the refractive index [3]. Takeshima et al. (2004) believed the refractive index change in glass was caused by local heat effects from phase separation [4], while Katayama (2002) proposed that all changes resulted from either: i) crosslinking, ii) phase separation, or iii) decomposition [5].

Recently a new process was discovered wherein existing molecules within a polymeric material become hydrophilic inside an intraocular lens (IOL) [6]. This change in hydrophilicity occurs when the polymeric material is immersed in an aqueous medium, and is exposed to femtosecond laser radiation. The aqueous medium and the femtosecond laser radiation provide the chemical basis for the hydrophilicity based refractive index change. After the exposure of the polymeric material, water slowly diffuses to the sites with increased hydrophilicity forming hydrogen bonds, typically over a 24 - 72 hour period of time, to create a negative refractive index change in the polymeric material.

Biomedical Optics EXPRESS

In this paper, the chemical and physical changes in an intraocular lens, which are caused by the exposure of the acrylic material to a femtosecond laser, are investigated. The acrylic material was tested by a number of different microscopic methodologies: Laser Induced Fluorescence (LIF) microscopy, Raman microscopy and Coherent Anti-Stokes Raman Scattering (CARS) microscopy, to determine the nature of the changes created in the material by the exposure to the femtosecond laser. The polar bonds within the acrylic material are altered such that the material absorbs additional water.

2. Technology background

2.1 Femtosecond laser induced refractive index change (RIS)

A new method for modifying the refractive index of polymeric materials has been developed, called Refractive Index Shaping (RIS) (Fig. 1(a)) [6]. High repetition rate femtosecond laser pulses are directed to a designated area to create a 'lens' inside an IOL. RIS changes the refractive characteristics of the polymeric material without cutting the material. The RIS-lens is a gradient lens, with the related refractive index change generated by the instantaneous energy of the laser pulse, which is regulated by an acousto-optical modulator (AOM) at approx. 1 MHz speed. The physical parameters of the procedure, like scan-speed, wavelength, pulse rate, energy per pulse, etc., are provided in [7], as well as data on the homogeneity of refractive index change. In preparation of a RIS lens, the femtosecond laser is directed to a small area within the polymeric IOL. The laser light has several effects on the acrylic material: (i) the most recognized is that the laser light heats the material and causes a change in the material as a result of the heat, and (ii) if the proper wavelength is utilized, the exposure to the laser light will alter the polarity of certain molecules within the polymeric material and change the hydrophilicity of the polymeric material. The change in hydrophilicity drives a large, repeatable and homogeneous change in refractive characteristics, which does not depend on the accumulation of heat and therefore can be used with a fast scan speed, allowing for in-vivo application.

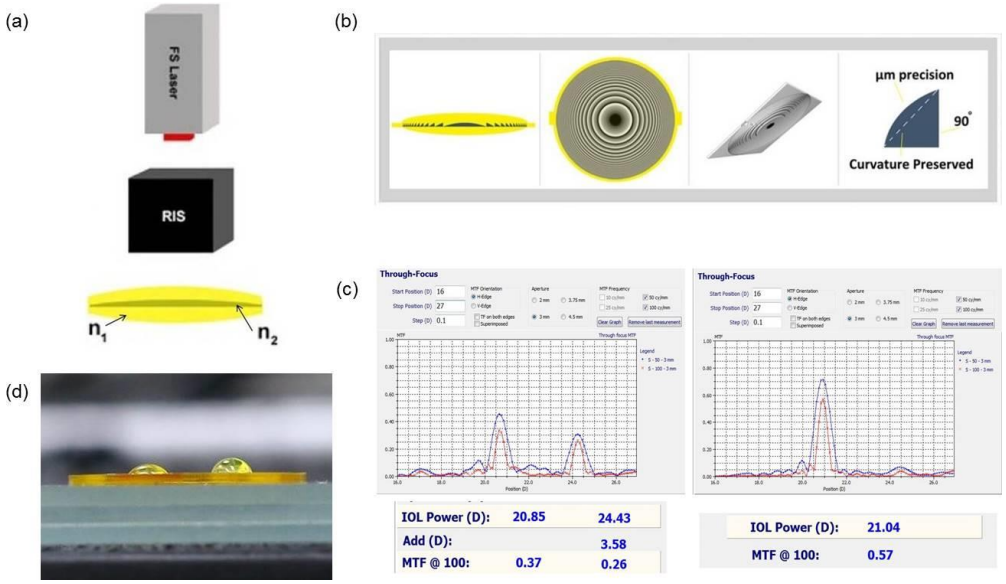

Fig. 1. (a) Refractive Index Shaping (RIS), Femtosecond (FS) laser, refractive index of IOL (n_1) and refractive index of RIS lens (n_2). (b) Phase Wrapping. (c) Multifocal IOL to Monofocal, before (left) and after (right) RIS-modification. (d) Hydrophilicity based Δn change.

Biomedical Optics EXPRESS

2.2 Phase wrapping

In a traditional convex lens, one would be limited to a height of 200 µm (central slab area) in order to adjust the optical power of the IOL. The power for a 6 mm lens with a height of 200 µm would be 0.44 dpt ($\Delta n = 0.01$). Phase wrapping is a process which is used to create a RIS "Lens" with enhanced diopter change, without increasing the height of the "Lens". Thus, a convex lens is reduced to a thin layer of approx. 50 µm thicknesses, creating multiple refractive zones. The different phase levels are created by controlling the energy per pulse and focal spot. For a "lens" with 6 mm diameter, one zone corresponds to 0.1 diopter (Fig. 1(b)).

2.3 Example of RIS-procedure: change of diffractive hydrophilic IOL into a monofocal IOL

The possibility of changing a diffractive multifocal IOL into a monofocal IOL was evaluated. A suitable lens design was created to match the diffractive power and energy split of the diffractive multifocal IOL, as depicted in Fig. 1(c). The original IOL measured 20.85 D with an add power of 3.58 D and a modulation transfer function (MTF) of 0.37 and 0.26. After RIS shaping, the IOL measured as a monofocal IOL at 21.04 D with an MTF of 0.57. The IOL shown in Fig. 1(c), before (left), was a commercial diffractive multifocal IOL. The RIS-process was imposed to change the lens from multifocal to monofocal [8]. The inverse process, i.e. creation of multifocality in a monofocal hydrophobic IOL is shown also in [8]. A RIS-lens can be 'erased', subsequentially, by e.g. creating a RIS-lens with opposite refraction in an adjacent layer.

2.4 Hydrophilicity based Δn change

To demonstrate that the hydrophilicity of the polymeric material has been changed, two areas of polymeric material were compared. One area of the material had not been treated, and the adjacent area was treated with the femtosecond laser. To test whether the treatment created a hydrophilic area, the wetting angle measurement technique was employed [9]. The treated and untreated sections of an acrylic hydrophobic material were exposed to a drop of water. Figure 1(d) (left) shows the drop of water on a treated area, while Fig. 1(d) (right) displays a water drop placed on an untreated area of the lens. The angle of the drop, on top of the treated material, in Fig. 1(d) (left), is ~64°, which indicates that it is in contact with a hydrophilic surface. The angle of the drop, on top of the untreated material, in Fig. 1(d) (right), is ~87°, which indicates that the drop is in contact with a hydrophobic surface. The change in hydrophilicity demonstrates that the treatment with a femtosecond laser created a hydrophilic area.

3. Materials and methods

Three different microscope setups have been used for the study: Laser Induced Fluorescence (LIF) microscopy (3.1) [10], Raman microscopy (3.2) [11] and Coherent Anti-Stokes Raman Scattering (CARS) microscopy (3.3) [12]. Various hydrophilic and hydrophobic intraocular lens materials were studied (3.4). Each microscope is being used to identify exactly what molecular changes occur upon exposure of the polymeric material to the light of the femtosecond laser.

3.1 Laser induced fluorescence (LIF) microscopy, STED-contrast

The STED (Stimulated Emission Depletion) microscope uses a low power pulsed supercontinuum laser source (WhiteLase SC450-PP-HE,Fianium, Southampton, UK) for excitation at virtually any optical wavelength. After removal of the IR part of the supercontinuum spectrum using a 760 nm short pass filter, the desired excitation wavelength is selected using an acousto-optical tunable filter (AOTF, PCAOM-VIS, Crystal

Biomedical Optics EXPRESS

Technologies, Palo Alto, USA). The beam passes the AOTF three times in order to suppress the undesired wavelength range of the supercontinuum spectrum; the triple pass suppresses 1000 times better than a regular single pass. The STED laser is a frequency-doubled pulsed fiber laser (Katana-08 HPKA/40/07750/600/1600/FS) providing 600 ps pulses of up to 40 nJ pulse energy at a wavelength of 775 nm. The STED laser can be triggered electronically over a wide frequency range (25/40 MHz) which greatly simplifies the synchronization of the excitation and STED pulses. The STED laser is triggered by the pulsed supercontinuum laser operating at 38.6 MHz.

3.2 Raman microscopy

Raman spectra were recorded on a commercial HORIBA XploRA PLUS Raman Microscope (HORIBA Jobin Yvon GmbH, Bensheim, Germany). All spectra were measured with a 10x objective with a 600 gr/mm grating. The wavelength of the continuous wave excitation laser source was 785 nm (with a laser output of approximately 100 mW). Raman spectra were acquired both in the fingerprint (200-1800 cm^{-1}) and high-wavenumber (2400-3800 cm^{-1}) regions.

3.3 Coherent anti-Stokes Raman scattering (CARS) microscopy

CARS images were acquired with a Leica TCS SP8 CARS system (Leica Microsystems, Mannheim, Germany). The picoEmerald laser (APE, Berlin, Germany) offering a fixed line of 1064.5 nm and a tuneable line from an optical parametric oscillator (780-940 nm) was coupled to a TCS SP8 confocal microscope. The laser combination of the fixed Stokes line and tuneable pump line allows detection of CARS signal in the vibration range of 1300-3400 cm^{-1}. A HC PL IRAPO 40x water immersion objective was used for the imaging and CARS signal was selected with a band path filter and detected with a non-descanned photon multiplier tube (PMT) detector at the transmitted light side.

The confocal capability of the system was used to take the overview images with fluorescence and bright field images of the samples. A HC PL APO 10x/0.40 CS objective was used. Images are stitched to the overview after multi-position scanning. Also the emission spectra at different excitation wavelengths were acquired with the TCS SP8 CARS system.

3.4 Materials

The microscopic study was performed on three different IOL materials. The following samples were studied: (1) hydrophilic acrylic material without yellow dye [13]: (1a) Hydrophilic acrylic intraocular lens (See e.g. paragraph 4.2.1) and (1b) Hydrophilic acrylic strip, cut from a hydrophilic acrylic button (See e.g. paragraph 4.2.2); (2) hydrophobic acrylic strip with yellow dye (blue blocking), cut from a hydrophobic acrylic button [14], and (3) hydrophobic acrylic strip without yellow dye, cut from a hydrophobic acrylic button [15]. The hydrophilic acrylic intraocular lens had a refractive power of 5 diopter, the strips were cubes of approximately 10 mm x 2 mm x 2mm dimension and exhibited no refractive power. All strips are made from buttons, with the material specified in [13], [14] and [15]. The acrylic buttons were disc shaped, 10 mm in diameter and 2mm thick.

The chosen microscopic techniques provide information of the chemical nature of the process, on the electronic (fluorescence) as well as the molecular (Raman) level. CARS-microscopy is sensitive to refractive index changes, due to the four-wave mixing feature. In case of the clear hydrophilic acrylic material, LIF microscopy, STED microscopy and Raman microscopy were applied. The yellow hydrophobic material as well as the clear hydrophobic material was studied with LIF microscopy, STED microscopy and CARS microscopy.

Biomedical Optics EXPRESS

4. Experimental results

4.1 Enhancement of hydrophilicity by femtosecond laser excitation

In Fig. 2, the photo-induced hydrolysis of polymeric material in aqueous media is presented, in which two hydrophilic functional groups, acid group and alcohol group, are produced. This result is similar to the results found in previous research on surface treatment of PMMA, with femtosecond laser two-photon excitation [16], and excimer laser UV-excitation [17].

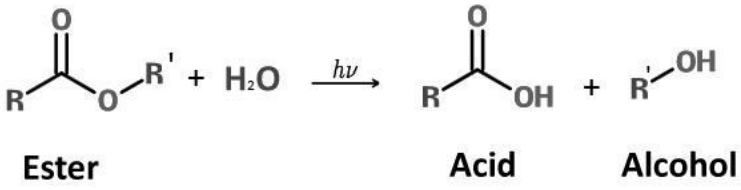

Fig. 2. Photo-induced Hydrolysis.

4.2 Femtosecond laser excited fluorescence in a hydrophilic intraocular lens

4.2.1 Section of a hydrophilic intraocular lens

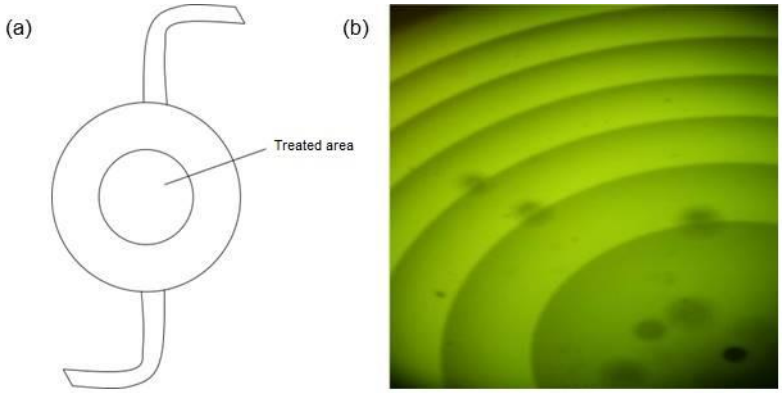

Fig. 3. (a) Schematic sketch of hydrophilic acrylic lens (5 diopters), RIS treated area 4mm circle in the center of the intraocular lens. (b) Fluorescence Image of a RIS-lens, inscribed in the hydrophilic acrylic lens, sketched in Fig. 3(a).

The schematic sketch of the hydrophilic intraocular lens of 5 diopters is shown in Fig. 3(a). The material is a clear material and measures 6 mm in diameter, and the treated area is within a 4 mm circle in the center of the lens. As shown in Fig. 3(b), the newly formed hydrophilic molecules in the laser treated area can be imaged by Laser Induced Fluorescence ("LIF") microscopy, visualizing the phase-wrapped RIS-lens by green fluorescent light emission, with blue excitation and wide field illumination (10x objective). Different shades of green correspond to different amounts of fluorescence light, indicating different amounts of newly formed hydrophilic polar molecules. The fluorescence image reflects the homogeneity and repeatability of refractive index change in the laser treated areas.

4.2.2 Hydrophilic strip

In Fig. 4(a), transmission (top) and fluorescence (bottom) images of a hydrophilic strip are depicted [13]. Two RIS lenses were created inside a hydrophilic strip of polymeric material, at the right and left side of the strip (Fig. 4(a), arrows). The detailed views of the strip imaged by Laser Induced Fluorescence (LIF) in Fig. 4(a) (bottom, arrows) and Fig. 4(b) shows the

Biomedical Optics EXPRESS

creation of hydrophilic areas exactly where the rings are located on Fig. 4(a) (top). In Fig. 4(c), an edge of the RIS-pattern in the hydrophilic strip is shown, and the homogeneity of refractive index change can be visualized on a micron-scale, imaged by the associated fluorescence of the newly created hydrophilic molecules.

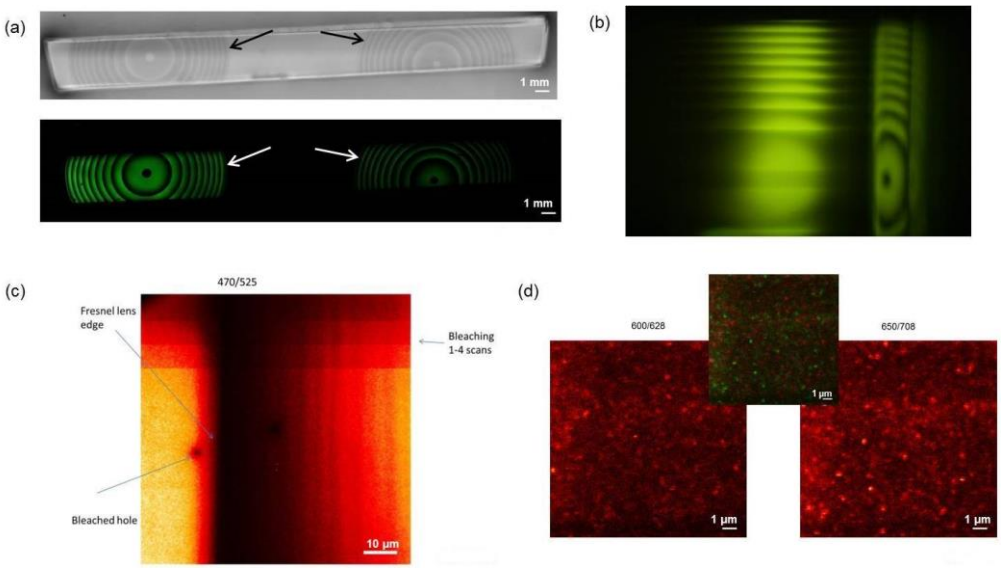

Fig. 4. (a) Hydrophilic Strip: transmission image (top) and fluorescence image (bottom) and the RIS-pattern indicated by arrows. (b) RIS-Pattern in Hydrophilic Strip (detail of left pattern of Fig. 4(a) bottom). (c) Edge of RIS-Pattern in Hydrophilic Strip (Zone boundary of Fresnel lens). (d) Simultaneous scans at 600 nm, resp. 650 nm excitation.

4.2.3 Fluorescent light, originating from newly created fluorophores (Simultaneous Scans)

In Fig. 4(d), the simultaneous scanning of a laser excited area with light of two different wavelengths, e.g. 600 nm (Left image, fluorescence detection at 628 nm) and 650 nm (Right image, fluorescence detection at 708 nm) is depicted, demonstrating the detection of spatially distributed fluorophores in "On/Off" states. When the fluorophore has exposure to light of the correct wavelength it absorbs energy and creates fluorescent light. This so-called "Blinking" indicates the presence of single fluorophores, with active or silent behavior. In the upper middle part, the two instantaneous images are overlaid, labeling the left image in red color and the right image in green color. Note the scale bar of 1 µm, demonstrating submicron resolution of the images. The regions imaged in Fig. 4(d) are only approx. 10 µm in size, and are selected in fully treated areas, resulting in homogeneous appearances.

The excitation/emission spectra of a laser excited area are plotted in a three dimensional graph, with the excitation wavelengths on the abscissa and the emission wavelengths on the ordinate (See Fig. 5(a)). The z-axis is depicting the intensity of the fluorescence light, emitted by the fluorophores. The fluorescence excitation and emission scan was done with a TCS SP8 X system (Leica Microsystems, Mannheim). Data analysis and the graphs were generated using the Leica confocal software LASX. The microscope was equipped with a white light laser. The highest fluorescence light emission was generated at a wavelength of 470 nm of the white light laser. The corresponding emission spectrum extends over a broad spectral region, from 500 nm to 650 nm, indicating the formation of hydrophilic polar molecules. This graph demonstrates the sensitivity of the polymer molecules to laser light excitation.

Biomedical Optics EXPRESS

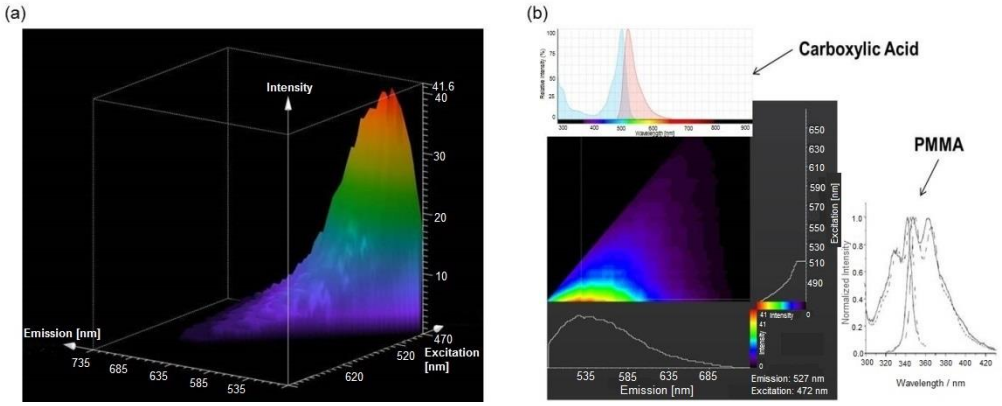

Fig. 5. (a) Excitation/Emission Spectra of fluorescent molecule. (b) Identification of fluorescent molecule.

4.2.4 Identification of fluorescent molecules as benzenamines

With an excitation wavelength of 472 nm, the emission spectrum of the fluorophore is centered at 527 nm, as depicted in the lower left of Fig. 5(b) (TCS SP8 X (Leica Microsystems GmbH)). In the upper left of Fig. 5(b), a typical excitation/emission spectrum of an aromatic carboxylic acid Rhodamine Green Carboxylic Acid is plotted for comparison, with excitation at 480 nm and emission centered at 525 nm. Thus, the spectral signature of the femtosecond laser generated polar molecule is similar to the characteristics of an aromatic carboxylic acid. Based on the chemical composition of the acrylic material with UV-dopant copolymer, the spectral signature of the femtosecond laser generated polar molecules points to the class of benzenamines, like N-phenyl-4-(phenylazo)-benzenamine ($C_{18}H_{15}N_3$). For comparison, the excitation/emission spectra of a pure acrylic material, e.g. PMMA, are shown on the lower right side, which are positioned in the deep UV, indicating that the UV-absorber molecules, which get excited by two-photon absorption, are essential to initiate the observed molecular changes.

4.2.5 Raman spectra of hydrophilic material (hydrophilic strip)

In Fig. 6, Raman spectra are depicted which were recorded at three different positions of the hydrophilic strip: Left (RIS-pattern, blue), Right (RIS-pattern, red), Center (Untreated area, black). The high wavenumber (2400-3800 cm^{-1}) region of the Raman spectra shown in Fig. 6(a) is dominated by two features. The sharp feature in the region 2800-3000 cm^{-1}, which is composed of three distinct vibrational bands, can be assigned to stretching vibrations of CH, and CH_2 functional groups [18]. The relatively broad feature ranging from 3100 cm^{-1} up to ca. 3600 cm^{-1} with a frequency maximum around 3300 cm^{-1} is characteristic for stretching vibrations of hydrogen bonded OH groups of water molecules in the hydrophilic polymer material [19]. The assignments of several distinct spectral features in the fingerprint region (200-1800 cm^{-1}), which are assigned in the Raman spectra of Fig. 6(b), indicate that the base material of the hydrophilic strip largely resembles the molecular structure of a poly-2-hydroxyethylmethacrylate (PHEMA) polymer [18, 20]. In the latter case the capability for the high water uptake of the material can be attributed to the presence of OH groups along the flexible polymer backbone, which can form primary hydrogen bonds with water molecules.

Biomedical Optics EXPRESS

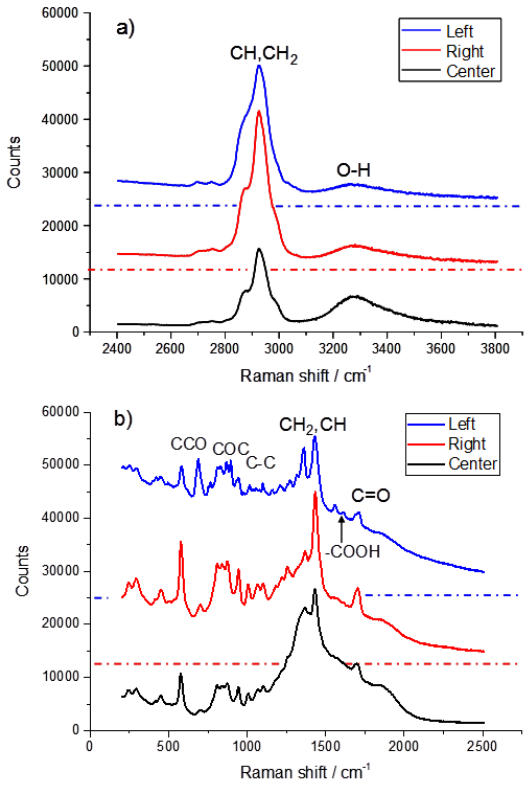

Fig. 6. Raman spectra of the hydrophilic strip: a) High-frequency part, b) Low-frequency part. Dashed dotted horizontal lines represent the zero signal base lines of the respective Raman spectra, which were shifted vertically for the sake of clarity.

As can be seen in Fig. 6(a) the overall OH band intensity is significantly diminished in the Raman spectra measured in the laser treated areas (Left and Right) as compared to the untreated area (Center) of the strip. This is consistent with consumption of H_2O molecules in the laser treated areas due to the photo-induced hydrolysis reaction shown in Fig. 2. Furthermore, the reduction of the OH band intensity in the laser treated region is paralleled by a significant increase of the CH and CH_2 stretching vibration band intensities, which further indicates reaction of the polymer material upon femtosecond laser treatment. The latter fact is confirmed by the observed significant change of the low frequency range Raman spectra (Fig. 6(b)) upon laser treatment. The Raman spectra taken within the treated area (Right, Left in Fig. 6(b)) exhibit a noticeable contribution of background fluorescence light in the low frequency region (200-2500 cm^{-1}), due to excitation/emission processes of newly created fluorophores. In contrast, there is almost no fluorescence background in the untreated area (Center in Fig. 6(b)), demonstrating, that fluorophores are solely generated by the irradiation with the femtosecond laser. Considering the possible presence of UV-blocker/stabilizers in the polymer material (such as e.g. benzotriazole derivatives [21, 22]) the newly created fluorescent molecules might be phenazine derivatives, which could be formed by reaction sequence initiated by the femtosecond two-photon laser induced photochemical activation of the benzotriazole copolymer derivatives. Again these molecules remain in their existing place and are modified by the exposure to the laser light. Furthermore, a new molecular vibration in the region 1600-1620 cm^{-1} that is observed in the laser treated area (Fig. 6(b), Left) which can be assigned to an aryl carboxylic acid COOH moiety [23]. This entity is a residual of the original reaction initiated by the laser light. The laser generated fluorophores could be phenazine-1- carboxylic acid molecules (see Table 1).

Biomedical Optics EXPRESS

Table 1. Spectral band assignments

Frequency in cm^{-1}	Possible assignments
550-610	CCO stretch
890-900	COC stretch
1080-1120	C-C stretch
1340-1375	CH_2 twist and rock
1400-1460	CH_2 in-plane bending, CH deformation
1600-1620	COOH stretch
1650-1750	C = O stretch
2800-3000	C-H stretch (of CH, CH_2 groups)
3100-3600	O-H stretch

4.2.6 Hydrophobic strip (yellow)

In Fig. 7(a), transmission (top) and fluorescence (bottom) images of a hydrophobic strip are depicted [14]. A RIS lens was patterned (Fig. 7(a)) in the center of the hydrophobic strip. The RIS pattern in the hydrophobic strip is indicated by the arrows in Fig. 7(a).

In Fig. 7(b), fluorescence spectra from the RIS-pattern of the yellow hydrophobic strip are shown, with excitation/emission at 405/500 nm, and 488/535 nm, respectively (TCS SP8 X (Leica Microsystems GmbH)).

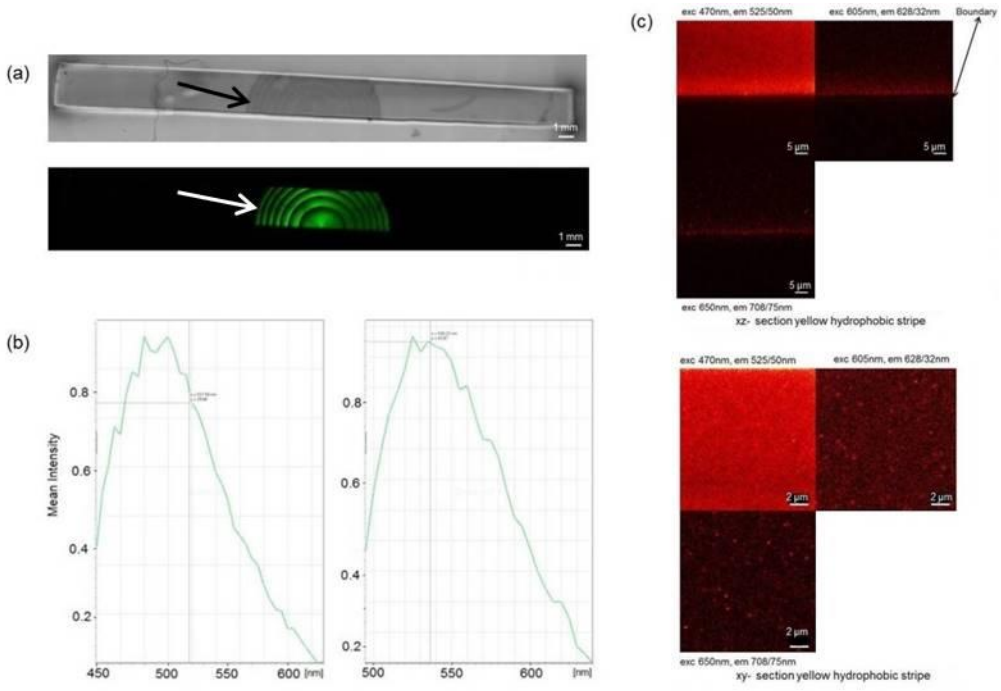

Fig. 7. (a) Hydrophobic Strip: transmission image (top) and fluorescence image (bottom) and the RIS- patterns are indicated by arrows. (b) Fluorescence spectra, excitation at 405 nm and emission max. at 500 nm (left), excitation at 488 nm and emission max. at 535 nm (right). (Sample: Yellow hydrophobic strip [14]). (c) Top: Magnified a few µm sized confocal xz-slice (side view) across a bright part of the Fresnel pattern. The samples physical boundary is where the intensity changes from bright (inside the sample) to dark region (outside the sample). Bottom: Magnified confocal xy-slice (top view, inside the sample) at a bright part of the Fresnel pattern. The fluorescence images were taken simultaneously at 470 nm, resp. 650 nm, resp. 650 nm excitation. Please note the scale bars.

Figure 7(c) (top) displays simultaneous xz-scans at three excitation wavelengths (exc 470 nm, em 525/50 nm (upper left), exc 605 nm, em 628/32 nm (upper right), exc 650 nm, em 708/75 nm (lower left). The fluorescence appeared strongest at 470 nm excitation. Inside the

Biomedical Optics EXPRESS

bulk material above the bright intensity edge the intensity drops after a few microns. This is probably caused by a mismatch of the refractive index between the immersion oil and the bulk material. Immersion oil was used for high resolution images and may produce artifacts in the images, as shown in Fig. 7(c).

Figure 7(c) (bottom) displays xy-sections of the fluorescence emissions taken at three wavelength bands (exc 470 nm, em 525/50 nm (upper left); exc 605 nm, em 628/32 nm (upper right); exc 650 nm, em 708/75 nm (lower left)). The xy scans were taken ca. 3 µm inside the yellow hydrophobic material. The fluorescence appears brightest with blue excitation. While the fluorescence appears homogenous at blue excitation, it exhibits brighter diffraction limited small spots above a homogenous fluorescence level in the red ranges. The spots are not co-localized in the two red channels. The images were taken quasi simultaneously in line multiplexing scanning mode. As discussed previously in the case of the clear hydrophilic material (see Fig. 4(d)), in the yellow hydrophobic material similarly spatially distributed fluorescent molecules in "On/Off" states are detected; this so-called "Blinking" indicates the presence of single fluorescent molecules, with active or silent behavior. The regions imaged in Fig. 7(c) are only approx. 10 µm in size, and are selected in fully treated areas, resulting in homogeneous appearances.

4.2.7 CARS-spectra, correlation CARS/fluorescence (yellow hydrophobic strip)

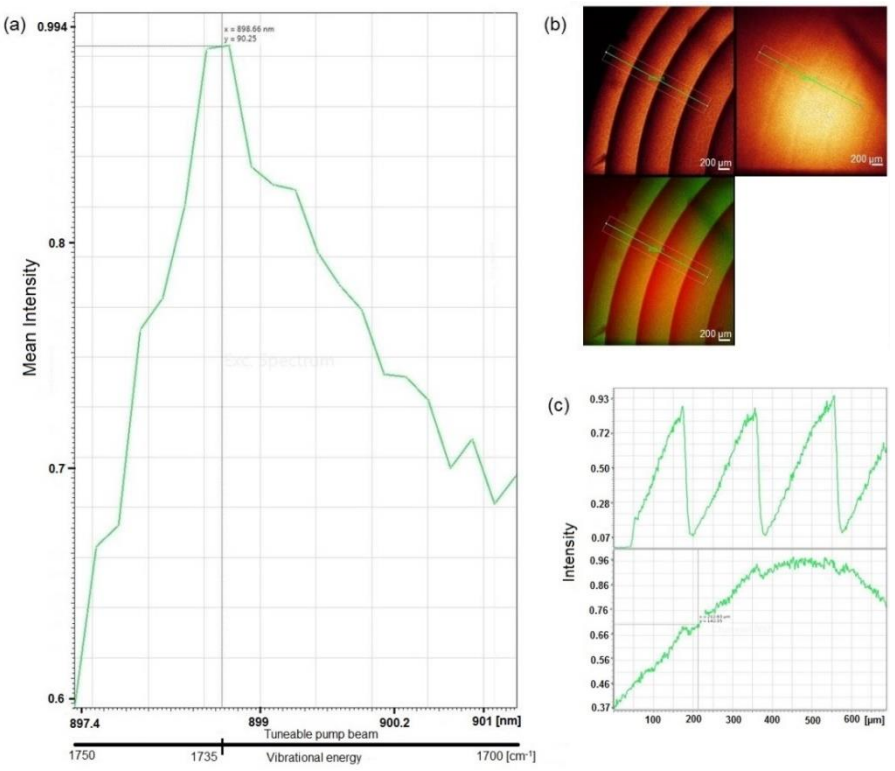

Fig. 8. (a) CARS-Spectrum yellow hydrophobic lens (1700-1750 cm^{-1}), max. at 1735 cm^{-1} (C = O molecular vibration (stretching mode)). (b) CARS (2954 cm^{-1}) and fluorescence images (TCS SP8 CARS, Leica Microsystems GmbH). (c) Correlation CARS and fluorescence cross-sections, yellow hydrophobic lens.

In Fig. 8(a), a CARS spectrum of the yellow hydrophobic strip is depicted, subtending the frequency range from 1700 cm^{-1} to 1750 cm^{-1}. The peak frequency amounts to 1735 cm^{-1}, indicating the C = O molecular vibration (stretching mode). On the abscissa, the tunable

Biomedical Optics EXPRESS

pump laser wavelengths are plotted (in nanometers), as well as the related vibrational mode frequencies (in wavenumbers cm^{-1}).

In Fig. 8(b), a CARS image, taken at a frequency of 2954 cm^{-1}, corresponding to CH/CH_2 molecular vibrations, is plotted in the upper right, with the fluorescence image in the upper left and the overlay of CARS/fluorescence images in the lower left. In Fig. 8(c), the cross-section profiles of the CARS (lower graph) and fluorescence (upper graph) signals along the lines indicated in Fig. 8(b) are plotted. The variation of the CARS signal is due to overlay mismatch of the pump and Stokes beams, generating the CARS signal, towards the edges of the image field, as can be seen from the color variances in the upper right image, shown in Fig. 8(b). The dips in the CARS signal at the zone boundaries of the Fresnel lens (see Fig. 8(c)), which can be recognized in the CARS image (Fig. 8(b), upper right), too, are essentially caused by a slight mismatch of the foci of the pump and Stokes beams at the zone boundaries, due to the refractive index step, imposed by the laser treated area of the IOL material.

4.2.8 Hydrophobic strip (clear)

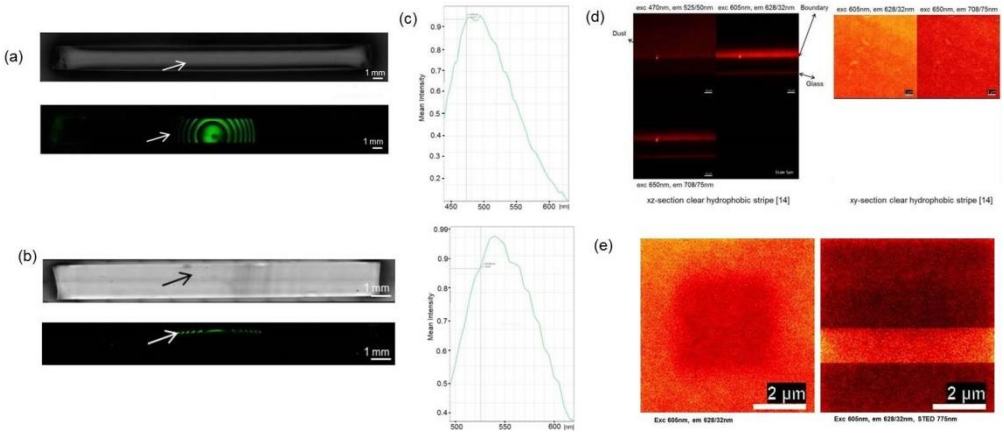

Fig. 9. (a) Hydrophobic clear strip (birdview): transmission image (top), fluorescence image (bottom) and the RIS-patterns indicated by arrows. (b) Hydrophobic clear strip (sideview): transmission image (top), fluorescence image (bottom). (c) Fluorescence spectra, excitation at 405 nm and emission max. at 500 nm (top), excitation at 488 nm and emission max. at 535 nm (bottom) (Sample: Clear hydrophobic strip [15]). (d) Left: Magnified a few µm sized confocal xz-slice (side view) across a bright part of the Fresnel pattern. Right: Magnified confocal xy-slice (top view, at the samples surface) at a bright part of the Fresnel pattern. The fluorescence images were taken simultaneously at 470 nm, resp. 605 nm, resp. 650 nm excitation. (e) High resolution fluorescence xy- images (top view) of clear hydrophobic strip. Left: The darker squared field shows an area which was previously scanned and gradually bleached. Right: The bright band indicates an area where the STED beam was switched off temporarily while the full image was scanned. Thus, the newly created fluorophores show analogous behavior (bleaching and stimulated emission) like regular fluorescent dyes. Please note the scale bars.

In Fig. 9(a) and 9(b), transmission (top) and fluorescence (bottom) images of a hydrophobic strip are depicted [15]. A RIS lens was patterned (Fig. 8(a) and 8(b), arrows) in the center of the hydrophobic strip.

In Fig. 9(c), fluorescence spectra from the RIS-pattern of the clear hydrophobic strip ([15]) are shown, with excitation/emission at 405/500 nm, and 488/535 nm, respectively. The spectra closely resemble the spectra from the RIS-pattern of the yellow hydrophobic strip [14], as well as the spectra from the hydrophilic strip [13], reaffirming the fact that similar fluorescent molecules are generated in three different materials.

Figure 9(d) (left) displays simultaneous xz-scans at three excitation wavelengths (exc 470 nm, em 525/50 nm (upper left); exc 605 nm, em 628/32 nm (upper right); exc 650 nm, em 708/75 nm (lower left)). The bright spot marks the surface of the clear hydrophobic material.

Biomedical Optics EXPRESS

The fluorescence appeared strongest at 605 nm excitation while it was very weak at blue excitation. Inside the bulk material the intensity drops after a few microns. This is probably caused by a mismatch of the refractive index between the immersion oil and the bulk material. The lower narrow line marks the coverslip glass surface on top of which the sample was mounted.

The clear hydrophobic material was imaged at two fluorescence bands simultaneously (see Fig. 9(d) (right)) (exc 605 nm, em 628/32 nm (upper left) and exc 650 nm, em 708/75 nm (upper right). The fluorescence emissions appear homogeneous in both wavelength bands at a diffraction limited resolution level of 230 nm. The regions imaged in Fig. 9(d) are only approx. 10 µm in size, and are selected in fully treated areas, resulting in homogeneous appearances.

The fluorescent molecules in the clear hydrophobic material bleach [15], i.e. photo-convert into a non-fluorescent species, upon excitation, similar to common organic fluorescent molecules. Figure 9(e) (left) shows a darker square region in the center, which was previously scanned several times. The regions imaged in Fig. 9(d) and 9(e) are only approx. 10 µm in size, and are selected in fully treated areas, resulting in homogeneous appearances.

The fluorescent species in the clear hydrophobic material can be stimulated from the excited to the ground state similar to common organic fluorescent molecules. Figure 9(e) (right) shows the fluorescence intensity measured in a STED microscope (See [10]), with excitation laser and STED laser simultaneously switched on. The brighter band shows a region where the STED laser was temporarily switched off. No finer structures could be found with STED imaging contrast. The noise is shot noise from a photon count per pixel of 17 in the bright region and a count of 6 in the regions where the STED laser was on.

4.2.9 CARS-spectra, correlation CARS/fluorescence (clear hydrophobic strip)

In Fig. 10(a), a CARS spectrum of the clear hydrophobic strip is depicted, subtending the frequency range from 1700 cm^{-1} to 1750 cm^{-1}. The peak frequency amounts to 1735 cm^{-1}, indicating the C = O molecular vibration (stretching mode). On the abscissa, the tunable pump laser wavelengths are plotted (in nanometers), as well as the related vibrational mode frequencies (in wavenumbers cm^{-1}).

In Fig. 10(b), a CARS image, taken at a frequency of 1720 cm^{-1} is plotted in the upper right, with the fluorescence image in the upper left and the overlay of CARS/fluorescence images in the lower left. In Fig. 10(d), the cross-section profiles of the CARS (lower graph) and fluorescence (upper graph) signals along the lines indicated in Fig. 10(b) are plotted. The variation of the CARS signal is due to overlay mismatch of the pump and Stokes beams, generating the CARS signal, towards the edges of the image field, as can be seen from the color variances in the upper right image, shown in Fig. 10(b). The dips in the CARS signal at the zone boundaries of the Fresnel lens (see Fig. 10(d)), which can be clearly recognized in the CARS image (Fig. 10(b), upper right), too, are essentially caused by a slight mismatch of the foci of the pump and Stokes beams at the zone boundaries, due to the refractive index step, imposed by the laser treated area of the IOL material.

In Fig. 10(c), a CARS image, taken at a frequency of 2954 cm^{-1}, corresponding to the CH/CH_2 molecular vibrations, (stretching mode), is plotted in the upper left, with the fluorescence image in the upper right and the overlay of CARS/fluorescence images in the lower left. In Fig. 10(e), the cross-section profiles of the CARS (lower graph) and fluorescence (upper graph) signals along the lines indicated in Fig. 10(c) are plotted. The variation of the CARS signal is due to overlay mismatch of the pump and Stokes beams, generating the CARS signal, towards the edges of the image field, as can be seen from the color variances in the upper left image, shown in Fig. 10(c). The dips in the CARS signal at the zone boundaries of the Fresnel lens (see Fig. 10(e)), which can be clearly recognized in the CARS image (Fig. 10(c), upper left), too, are essentially caused by a slight mismatch of

Biomedical Optics EXPRESS

the foci of the pump and Stokes beams at the zone boundaries, due to the refractive index step, imposed by the laser treated area of the IOL material, affecting the pump and Stokes beam differently, due to dispersion.

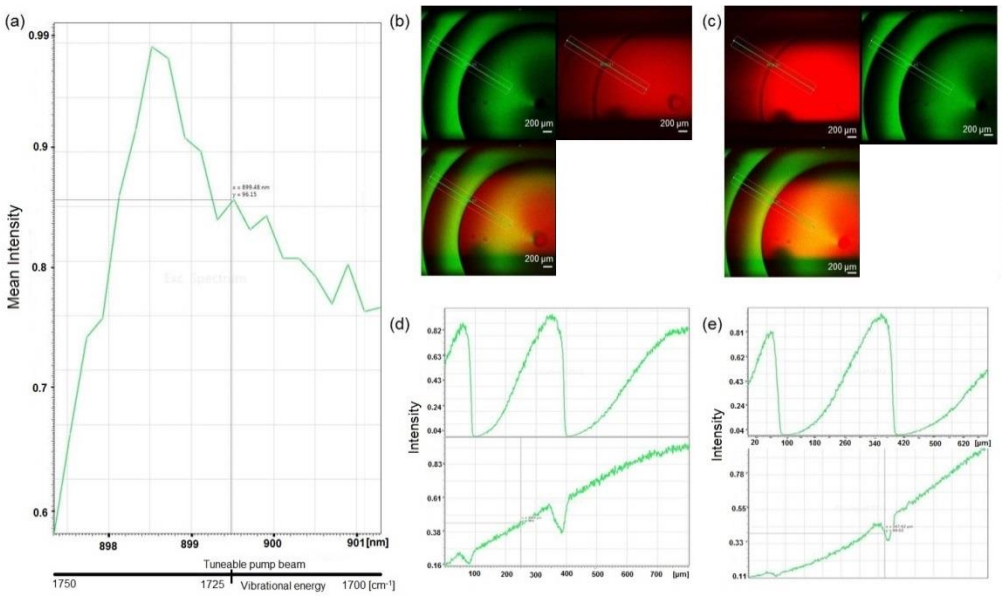

Fig. 10. (a) CARS-Spectrum clear hydrophobic lens (1700-1750 cm^{-1}), max. at 1735 cm^{-1} (C = O molecular vibration). (b) CARS (1720 cm^{-1}) and fluorescence images (TCS SP8 CARS, Leica Microsystems GmbH). (c) CARS (2954 cm^{-1}, CH/CH_2 vibrational mode) and fluorescence images (TCS SP8 X (Leica Microsystems GmbH)). (d) Correlation CARS (C = O mode) and fluorescence cross-sections, clear hydrophobic lens. (e) Correlation CARS (CH/CH_2 mode) and fluorescence cross-sections, clear hydrophobic lens.

5. Discussion and conclusion

The RIS treatment (see e.g. Fig. 1(a)) uses a femtosecond laser to change the hydrophilicity of the targeted area, which allows a change in the refractive index, e.g. a negative refractive index change in the laser treated areas. This effect in combination with a two dimensional scan pattern allows the creation of a refractive or diffractive lens inside the material.

The hydrophilicity increase is facilitated by photo-induced hydrolysis of polymeric material in aqueous media. Among many possible mechanisms, the transformation of the ester group into an acid group and an alcohol group may be involved; thus, the ester group produced two hydrophilic functional groups increasing the hydrophilicity of the treated polymer. The spectral signature identifies one of the femtosecond laser generated polar molecules as benzenamines, like N-phenyl-4-(phenylazo)-benzenamine ($C_{18}H_{15}N_3$). Furthermore, the Raman spectra indicate, that another laser generated fluorophore could be phenazine-1-carboxylic acid ($C_{13}H_8N_2O_2$) molecules. Since the femtosecond laser treatment of the lens material was conducted in aqueous media, water molecules are available for photo-induced hydrolysis of the ester. The hydrogen bonding between water molecules and the hydrophilic groups of acid and alcohol is well established. As a result, the refractive index (RI) of the treated polymer is between the RI of the untreated polymer (1.49) and the RI of water of 1.33.

Our experimental findings, with regard to emission of fluorescent light in the laser-treated areas in polymeric materials, closely resemble coloring effects in glass-materials, which are exposed to high doses of femtosecond laser radiation [24–28]. As shown above, the irradiation with femtosecond laser pulses can induce considerable absorption in polymeric

Biomedical Optics EXPRESS

materials at the visible spectral region. In glass, at femtosecond laser fluences close to the dielectric breakdown (approx. 10 J/cm^2), the formation of color centers is observed. Electrons and holes are generated due to the nonlinear excitation of the material by femtosecond laser pulses [29, 30]. A model was developed [24], associating the excitations created initially by the femtosecond laser to the formation of Frenkel excitons, which comprise localized electron-hole pairs. In contrast to glass, the polymeric material is doped with UV-absorber molecules which are excited by two-photon processes, generating hydrophilic molecules, and instilling the observed emission of fluorescent light.

In conclusion, a photochemical process was identified, wherein hydrophilic polar functional groups are generated by photo-induced hydrolysis of polymeric material, in areas which are exposed to a femtosecond laser, thus providing the chemical basis for a hydrophilicity based negative refractive index change, facilitating the creation of a RIS-lens. The newly formed functional groups, e.g. amines and carboxylic acids, are strongly hydrophilic. The molecules are monomers or dimers, embedded in the original polymer and the UV-absorber co-polymer. These molecules remain in their existing place and are modified by the exposure to the laser light. In three different polymeric materials, fluorophores with identical spectral signatures were detected. Thus, photo-induced hydrolysis results in rearrangements of chemical bonds, essentially within the UV-absorber molecule, preserving the integrity of the polymeric material. Based on the fluorescence, Raman and CARS spectra, no leachables are generated. Also, standard leachables-tests have been performed on RIS-modified IOLs, and no leachables were found.